HAL open science

Simulation of free fall and resonances in the GOCE mission

Aleš Bezděk, Jaroslav Klokočník, Jan Kostelecký, Rune Floberghagen, Christian Gruber

► To cite this version:

Aleš Bezděk, Jaroslav Klokočník, Jan Kostelecký, Rune Floberghagen, Christian Gruber. Simulation of free fall and resonances in the GOCE mission. Journal of Geodynamics, 2009, 48 (1), pp.47. 10.1016/j.jog.2009.01.007 . hal-00542925

HAL Id: hal-00542925

https://hal.science/hal-00542925

Submitted on 4 Dec 2010

HAL is a multi-disciplinary open access archive for the deposit and dissemination of scientific research documents, whether they are published or not. The documents may come from teaching and research institutions in France or abroad, or from public or private research centers.

L'archive ouverte pluridisciplinaire **HAL**, est destinée au dépôt et à la diffusion de documents scientifiques de niveau recherche, publiés ou non, émanant des établissements d'enseignement et de recherche français ou étrangers, des laboratoires publics ou privés.

Accepted Manuscript

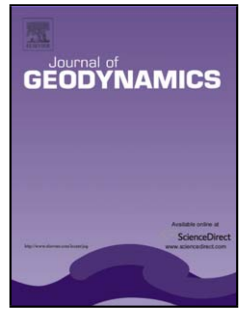

Title: Simulation of free fall and resonances in the GOCE mission

Authors: Aleš Bezděk, Jaroslav Klokočník, Jan Kostelecký, Rune Floberghagen, Christian Gruber

PII:	S0264-3707(09)00027-1
DOI:	doi:10.1016/j.jog.2009.01.007
Reference:	GEOD 879
To appear in:	*Journal of Geodynamics*
Received date:	29-10-2008
Revised date:	27-1-2009
Accepted date:	27-1-2009

Please cite this article as: Bezděk, A., Klokočník, J., Kostelecký, J., Floberghagen, R., Gruber, C., Simulation of free fall and resonances in the GOCE mission, *Journal of Geodynamics* (2008), doi:10.1016/j.jog.2009.01.007

This is a PDF file of an unedited manuscript that has been accepted for publication. As a service to our customers we are providing this early version of the manuscript. The manuscript will undergo copyediting, typesetting, and review of the resulting proof before it is published in its final form. Please note that during the production process errors may be discovered which could affect the content, and all legal disclaimers that apply to the journal pertain.

ACCEPTED MANUSCRIPT

Simulation of free fall and resonances in the GOCE mission

Aleš Bezděk*[,a], Jaroslav Klokočník[a], Jan Kostelecký[b], Rune Floberghagen[c], Christian Gruber[a]

[a]*Astronomical Institute, Academy of Sciences of the Czech Republic, Fričova 298, 251 65 Ondřejov, Czech Republic*
[b]*Research Institute of Geodesy, Topography and Cartography, Ústecká 98, 250 66 Zdiby, Czech Republic*
[c]*ESA/ESRIN, Via Galileo Galilei, 00044 Frascati, Italy*

Abstract

GOCE, ESA's first Earth gravity mission, is currently to be launched early in 2009 into a sun-synchronous orbit. Using the full-scale numerical propagator, we investigated the satellite's free fall from the initial injection altitude of 280 km down to the first measurement phase altitude (at 264 km). During this decay phase the satellite will pass below the 16:1 resonance (268.4 km). The effect of this resonance, together with the uncertainty in the solar activity prediction, has a distinct impact on the evolution of the orbital elements. Then, to maintain a near-constant and extremely low altitude for the measurement operational phases, the satellite will use an ion thruster to compensate for the atmospheric drag. In order to obtain the groundtrack grid dense enough for a proper sampling of the gravitational field, ESA set constraints for a minimum groundtrack repeat period. We studied suitable repeat cycles (resonant orbits) in the vicinity of 16:1 resonance; we found that

*Corresponding author, tel.: +420 323620232, fax: +420 323620117.
Email address: bezdek@asu.cas.cz (Aleš Bezděk)

Preprint submitted to Journal of Geodynamics *January 27, 2009*

ACCEPTED MANUSCRIPT

they differ greatly in stability towards small perturbations of the satellite's mean altitude and in temporal evolution of the groundtrack coverage. The results obtained from the usual analytical treatment of orbital resonances were refined by more realistic numerical simulations. Finally, we formulated suggestions that might be useful in GOCE orbit planning.

Key words: GOCE, orbital propagator, orbital resonance, repeat orbit, groundtrack coverage

1. Introduction

The Gravity field and steady-state Ocean Circulation Explorer Mission (GOCE) is to date the most advanced gravity space mission, the first Core Earth Explorer mission of the European Space Agency's (ESA's) Living Planet programme. After a few postponements, the satellite is about to be launched in February 2009 from the Plesetsk Cosmodrome in Russia into a low altitude sun-synchronous orbit (the situation by the time when the manuscript was finalized). The satellite will carry a gradiometer, an instrument composed of three pairs of highly sensitive microaccelerometers that measure components of the gravitational acceleration in three dimensions, from which the Marussi tensor of the second derivatives of the gravitational potential is to be calculated (e.g. Hofmann-Wellenhof and Moritz, 2006). The data collected are expected to significantly improve the global models of the Earth gravitational field and to provide a high-resolution map of the geoid. Apart from geodesy and positioning, a host of applications are expected in geophysics, oceanography, climatology and other geosciences. For in-depth information about the project, refer to ESA's website,

Accepted Manuscript

ACCEPTED MANUSCRIPT

http://www.esa.int/goce/.

The objective of this paper is to study two subjects connected with the GOCE mission profile: the free fall in the early orbit phase and the groundtrack repeatability during the measurement operational phases. The mission is divided into several phases (see, e.g. Drinkwater et al., 2007; ESA, 1999, 2004), which may be summarized as follows. The GOCE satellite will be injected into a dusk-dawn nearly sun-synchronous orbit to guarantee a stable and near-constant energy supply from the solar panels. *Sun-synchronicity* of the orbit means that the orientation of the satellite orbital plane is constant relative to the direction to the Sun (projected onto the equatorial plane). The *dusk-dawn* attribute says that the local time at the ascending node is 18 hours, thus the orbital plane, within which the satellite circles around the Earth, will remain approximately perpendicular towards the Sun direction. From the injection altitude of 280 km, the satellite will be controlled to slowly decay down to 264 km, while the spacecraft instruments will be checked out and calibrated. The scientific requirements of the near-constant measurement altitude dictate the orbit to be circular; the sun-synchronicity condition determines the orbital inclination, 96.7°. Under such conditions, the satellite's fully sunlit trajectory will be affected by seasons of short eclipses (duration less than 10 min per orbit) and long eclipses (less than 30 min per orbit). Two, or possibly three, measurement operational phases are planned, each occupying 3–7 months, interrupted by a hibernation mode during the long eclipse seasons. The requirement for the groundtrack repeat period of GOCE to be equal or larger than two months results in the maximum separation of groundtracks less than 42 km.

Accepted Manuscript

ACCEPTED MANUSCRIPT

2. Free fall of GOCE

The higher injection altitude and the subsequent free fall phase of GOCE is intended to correct potential launch injection errors in the desired orbital elements for the first measurement operational phase (MOP1); also, during the free fall phase the ion propulsion unit and the gradiometer will be checked out. In our simulation of such a fall, we tried to model all important orbital perturbative accelerations; we made use of the numerical propagator NUMINTSAT (Sec. 2.1). The aim was to get a reliable prediction of the orbital evolution and especially of the period needed for the satellite to descend down to the MOP1 altitude, where the drag compensation system will be activated to maintain this altitude. This prediction depends notably on the uncertainty in solar activity prediction and on the used physical characteristics of the spacecraft.

Figure 1 should be positioned here.

At the time of writing the manuscript, the supposed launch date was 10 November 2008, 14:21 UTC. The simulated orbital evolution of the GOCE satellite, modelled as a passive freely falling body, is in Figure 1. A manifest feature of the graphs is the steady decrease in the satellite's semimajor axis (upper left panel) or equivalently mean altitude (lower right panel). By *mean altitude* we designate here, and henceforth, the mean semimajor axis with the Earth equatorial radius (R_e=6378.1363 km) subtracted. This decrease in altitude is caused by atmospheric drag, which limits the lifetime of satellites

Accepted Manuscript

ACCEPTED MANUSCRIPT

in low Earth orbits by making them finally burn up in denser layers of the atmosphere.

The two curves labelled as *'nominal'* correspond to the nominal *satellite attitude*, when the side with the smallest cross-section is ahead in the direction of motion. The curves labelled by '15° tilt' show the orbital evolution of the satellite body, when it is slightly *tilted* relative to the velocity vector. When tilted, the spacecraft's cross-sectional area with respect to the impinging air particles is augmented, atmospheric drag is increased, and the satellite loses altitude more quickly. In Fig. 1, this is clearly visible in the evolution of semimajor axis and mean altitude.

The second label 'max' or 'min' (of curves in Fig. 1) refers to the maximum or minimum predicted level of *solar activity*. One of the physical quantities determining the value of atmospheric drag is the atmospheric density, which in turn depends on the level of solar activity in UV. Solar activity in UV changes periodically over the well-known 11-year period (sunspot cycle). Unfortunately, it is not possible to predict the future time evolution of solar activity precisely enough, which may introduce a considerable amount of uncertainty in longer orbital predictions (months and more). This uncertainty due to solar activity is also evident on the hypothetical lifetime predictions for GOCE in Fig. 1, would the spacecraft be left freely falling without the activation of the drag compensation system.

Due to a delayed start of the new cycle of solar activity (Biesecker et al., 2008; NOAA, 2007), it seems feasible that the first measurement phase will take place below the 16:1 resonance located at 268.4 km (lower right panel of Fig. 1). A passage through an orbital resonance may cause a considerable

ACCEPTED MANUSCRIPT

variation in the orbital elements, most visible as *quasi-secular change in inclination* (upper right panel of Fig. 1). Around the time of passing through the strong 16:1 resonance, the inclination may undergo negative or positive quasi-secular changes depending on the specific values of orbital elements. The exact date of 16:1 passage is apparent in Fig. 1, at day 31 for the red curve labelled 'nominal; max' and especially at day 45 for the green curve 'nominal; min', when the quasi-secular changes in inclination are significant compared to the usual periodical variations due to odd zonal harmonics. As is apparent in Fig. 1, the quasi-secular change in inclination under the 16:1 resonance may occur ±15 days relative to the exact date of passage (more on resonances in Sec. 3).

Our predictions were compared with predictions provided by ESA for one of the previous launch dates. Apart from solar activity, another parameter having direct influence on the atmospheric drag is the so-called *drag coefficient*. We adopted the proposed higher value of the drag coefficient for the 15° tilt scenarios, which enhances the rate of altitude decrease (lower right panel of Fig. 1). After this modification, we obtained comparable results for the time of the satellite descent from the injection altitude to the MOP1 orbit. The graphs in Fig. 1 were obtained using the ESA values for the drag coefficient: 4.5 for the 'nominal' curves, 6.3 for the '15° tilt' ones.

2.1. Orbital propagator NUMINTSAT

For the free fall simulation of GOCE we made use of the NUMINTSAT orbital propagator, which is based on the numerical solution of the second-order differential equations of motion using the explicit Runge-Kutta method of order 8 due to Dormand and Prince (Hairer et al., 1993). The purpose of

ACCEPTED MANUSCRIPT

NUMINTSAT is to simulate precise orbits of satellites in low Earth orbits (LEO; altitudes of 100–2000 km). In this section we want to give a brief overview of the perturbative accelerations acting on LEO satellites such as GOCE, as they are modelled by the NUMINTSAT propagator.

Figure 2 should be positioned here.

To illustrate the character of the individual perturbative accelerations, in Figure 2 we have plotted the histograms of the absolute values of accelerations encountered by GOCE. During the simulation of a one-year long orbit, we recorded the perturbative accelerations acting on the spacecraft at fixed time intervals of 20 minutes. The three panels correspond to the axes of the local reference frame, whose origin is at the spacecraft gravity centre, the *along-track* component lies in the direction of the satellite velocity, *cross-track* is collinear with the orbital kinetic momentum (normal to the orbital plane) and (quasi) *radial* direction completes the two preceding vectors. In order to show the strength of the individual perturbations in each component, we took the absolute values of the accelerations and divided them into magnitude classes over logarithmic scale. In this way we obtained a separate histogram (frequency distribution) for each perturbation. We do not show the actual counts on the y-axis (which is linear), as these are only formal depending on the sampling period and would add complexity to the graphs.

The dominant *central attraction term* due to the Earth gravity (labelled by 'GRAV μ/r' in Fig. 2) is located mainly in the radial direction because of the near circularity of GOCE's orbit, where its value reaches $9.02\ \mathrm{m\,s^{-2}}$.

Accepted Manuscript

ACCEPTED MANUSCRIPT

In case of only central force action, the satellite's orbit would be an ellipse invariable in its shape and orientation (Keplerian ellipse). The main perturbation to this ideal 2-body problem is the *acceleration due to oblateness* ('GRAV J2'). It is apparent in all three components, its value being roughly three orders of magnitude less than that of the central attraction. In the spherical harmonic expansion of the geopotential, the Earth's oblateness is quantified by the second zonal harmonic coefficient, J_2. The next largest perturbation, less by one to two orders of magnitude than the previous one, is caused by a composite effect of *higher degree and order geopotential terms* ('GRAV rest'), the largest of them being due to the third zonal harmonic, J_3 (pear-shape of the Earth).

Other *perturbations of gravitational origin*, of magnitudes 10^{-8}–$10^{-6}\,\mathrm{m\,s^{-2}}$, present in all the components, are due to the attraction of the Sun and Moon ('LUNISOL'), to solid Earth tides ('SE_TIDE') and to ocean tides ('OC_TIDE'). The last depicted gravitational perturbation comes from the general theory of relativity ('RELATIV') and its most important action is in radial direction.

Now, we will describe the *nongravitational perturbations*, whose common feature is that they depend on the physical characteristics of the spacecraft, namely on its mass and shape; for that reason they are also called *surface forces*. *Atmospheric drag* ('DRAG') is present mainly in along-track direction, where it reduces the total energy of the satellite, but it is also visible in the cross-track component. GOCE's ion thruster will counterbalance the main along-track component of drag. Finally, we consider the accelerations produced by *radiation pressures*. The largest among them is the direct so-

ACCEPTED MANUSCRIPT

lar radiation pressure ('DSRP'), which is present in all components, when the satellite is sunlit. A special feature is a peak of almost constant size in cross-track direction brought about by the dusk-dawn character of the GOCE sun-synchronous orbit. While the reflected solar radiation ('ALB') is only faintly visible in radial component, the same magnitude range 10^{-9}–10^{-8} $\mathrm{m\,s^{-2}}$ occupies the terrestrial infrared radiation ('IR'), which acts in radial component also at night.

3. Resonances and groundtrack coverage

An *orbital resonance* $R{:}D$ occurs, when the satellite performs exactly R nodal revolutions, while the Earth rotates D times with respect to the satellite's precessing orbital plane, R and D being coprime integers (i.e. they have no common factor other than 1). Or equivalently, a *groundtrack repeat orbit* has a groundtrack that repeats after an integer number R of orbital revolutions and an integer number D of nodal days, where a nodal day is the period between recurrence of the ascending node over the same Earth-fixed meridian. Because the precession of the node is much slower than the Earth's rotation rate, a nodal day differs only slightly from a solar day, and in case of a sun-synchronous orbit, they are equal. In the following, we will use the terms 'resonant orbit' and 'repeat orbit' interchangeably.

Resonant orbits have become noteworthy in the study of artificial satellites dynamics since the 1970's, e.g. to evaluate the lumped geopotential harmonic coefficients (e.g. Gooding et al., 2007; King-Hele, 1992; King-Hele and Winterbottom, 1994; Klokočník et al., 2003) or in the mission planning for Earth observing satellites, where the groundtrack repeat is a significant

ACCEPTED MANUSCRIPT

characteristic of the orbit (Colombo, 1984; Parke and Born, 1993; Parke et al., 1987). In the GOCE mission, the scientific requirements stipulate a gravity field sampling at very low, constant altitude with a global and uniformly distributed dense groundtrack coverage, which leads to a repeat period equal to or larger than 2 months (ESA, 1999). The choice of the operational altitude is determined by the performance of the onboard ion thruster to eliminate the air drag, and actually it seems feasible to place GOCE below 16:1 resonance (Fig. 1). In this section we will discuss repeat orbits suitable for the GOCE mission using both the linear and numerical orbit simulation.

Analytical treatment of orbital resonances is based on the effects of the largest gravitational perturbation due to Earth oblateness. In terms of classical orbital elements, the second zonal term of the geopotential causes the well-known secular changes in right ascension of the ascending node, Ω, argument of perigee, ω, and mean anomaly, M, (see e.g. Kaula, 1966; Zarrouati, 1987)

$$\dot{\Omega} = -\frac{3}{2} n J_2 \left(\frac{R_e}{a}\right)^2 \cos i \; (1-e^2)^{-2} \,, \tag{1}$$

$$\dot{\omega} = -\frac{3}{4} n J_2 \left(\frac{R_e}{a}\right)^2 (1 - 5\cos^2 i) \; (1-e^2)^{-2} \,, \tag{2}$$

$$\dot{M} = n - \frac{3}{4} n J_2 \left(\frac{R_e}{a}\right)^2 (1 - 3\cos^2 i) \; (1-e^2)^{-3/2} \,, \tag{3}$$

where n is mean motion. In terms of mean elements, where the short-period variations over one satellite revolution are averaged out, the Earth oblateness causes the orbital plane to precess at a constant rate $\dot{\Omega}$, and the perigee to circulate at the rate given by $\dot{\omega}$. According to the above definition of resonance, using the nodal period of the satellite, $2\pi/(\dot{\omega}+\dot{M})$, and the nodal day, $2\pi/(\omega_e - \dot{\Omega})$, where ω_e is the angular rate of the Earth, neglecting the terms in e^2, we obtain (Klokočník et al., 2003)

$$n = \omega_e \frac{R}{D} \left\{ 1 - \frac{3}{2} J_2 \left(\frac{R_e}{a} \right)^2 \left(4\cos^2 i - \frac{R}{D}\cos i - 1 \right) \right\} . \tag{4}$$

For a given inclination, which in case of GOCE results from sun-synchronicity, and for a pair of coprime integers R and D, equation (4) may be used to find a semimajor axis for a corresponding resonant orbit. These resonant orbits are shown in Figure 3 as red points. In accordance with the ESA's above mentioned constraint of at least 2-month repeat period, we chose two 61-day repeat orbits, possible candidates of the GOCE measurement phase orbits, for more detailed analysis. For an R:D resonant orbit, after the repeat period has been completed, the grid of groundtracks should theoretically be homogeneous with an equatorial *node separation*

$$\Delta\lambda^{(deg)} = 360°/R \quad \text{or} \quad \Delta\lambda^{(km)} = 2\pi R_e/R \; . \tag{5}$$

Thus, after 61 nodal days, the difference in density of groundtrack coverage between the repeat orbits 977:61 and 978:61 is very small, with the equatorial node separation of 0.3685° (41.02 km) and 0.3681° (40.98 km), respectively. Yet, apart from the obvious 4.5-km difference in mean altitudes (Fig. 3), the two repeat orbits do differ from, say, a practical point of view, in temporal evolution of the groundtrack coverage and in stability towards small perturbations of the mean altitude.

Figure 3 should be positioned here.

ACCEPTED MANUSCRIPT

Figure 4 should be positioned here.

3.1. Evolution of groundtrack coverage

Figure 4 shows the temporal evolution with which the groundtracks cover the Earth surface for the two resonant orbits discussed above. The groundtrack grid of the higher orbit 977:61 is laid down in a homogeneous way over the whole repeat period, consecutively filling up two large gaps on the equator (left column of panels in Fig. 4). On the contrary, the groundtrack grid of the lower repeat orbit 978:61 is created in two phases: after the first 30 days the surface is almost homogeneously covered by a half density grid, and then, during the second 30 days, the full structure of the 978:61 homogeneous grid is completed (right column of panels in Fig. 4). In fact, after the first 30-day period, the node separation of the half-filled 978:61 grid is very close to that of the 481:30 repeat orbit, a 30-day repeat cycle with an altitude very close to that of the 978:61 orbit (Fig. 3).

3.2. Necessary adjustment of semimajor axis to obtain groundtrack repeat

The reader might have noticed a small difference in the mean altitudes of the 977:61 repeat orbit in Figures 3 and 4, and in those of the 978:61 repeat orbit. When we started to draw histograms of node separation for the two repeat orbits in order to visualize their possibly diverse characteristics, for the lower 978:61 orbit we obtained a double peaked graph of shape similar to two red bars in Fig. 5. These results were produced by analytical as well as by numerical orbit propagators (and also by ESA's simulator of GOCE's orbit). But according to the simple theoretical evaluation (Eq. 5), after the repeat

Accepted Manuscript

ACCEPTED MANUSCRIPT

period is elapsed, such a histogram should produce a single peak, maybe spread around the central value $360°/R$, but certainly not two distinctly separated peaks. In this section, we will give an explanation to this problem, and derive results, which might be useful for the GOCE measurement altitude selection.

Figure 5 should be positioned here.

3.2.1. Histograms based on analytical orbit theory

Let us first model and analyze the resonant orbits using a simple analytical theory with only J_2 perturbative term using the formulas from Tapley et al. (2004, pp. 493–497). The theory conforms to near-circular orbits, where the classical elements e and ω fail to be mathematically well defined, by replacing e and ω with nonsingular elements, $h = e \sin \omega$, $k = e \cos \omega$. It is a first-order theory in J_2 based on the original Brouwer (1959) paper.

In Figure 5, the J_2 theory was used to produce histograms of node separation for the lower repeat orbit 978:61 over the completed 61-day repeat period. Each time we simulated the orbit with the specified mean altitude and collected all the longitudes of the ascending nodes; gradually these ascending nodes reduce the gaps in longitude on the equator, as is shown in Fig. 4. Recall that the context of using the repeat orbits for GOCE is that we need no equatorial gaps larger than 42 km (or equivalently 0.377°), as they are places with no direct overflight of the satellite; therefore, we are interested in the overall distribution of lengths of these gaps, after the proposed 61-day

ACCEPTED MANUSCRIPT

repeat period is over. For this purpose we sorted the collected ascending node longitudes and took their differences; in such a way we obtained the separations between the successive ascending nodes and could draw their histogram for each particular simulation. To refer to the length of the equatorial gaps, we will use the term equatorial node separation defined previously.

At the centre of the upper panel of Fig. 5, the blue bar is located at the angular node separation $\Delta\lambda \simeq 0.368°$ corresponding to an exact 978:61 repeat orbit, according to Eq. (5). We obtained this single-peaked histogram by using the mean altitude of 259.38 km, as is indicated above the bar. Next, we reduced the mean altitude by 50 metres, and used the data from the analytical theory to produce the histogram of node separation, which has two distinct green bars at 0.246° and 0.490°. For the mean altitude of 259.33 km, one can find a corresponding resonant configuration in Fig. 3, whose repeat period is 152 days: in this case, the regular groundtrack grid is not yet finished and the histogram has two peaks (cf. the middle right panel of Fig. 4). The histogram with the bars in cyan, and the mean altitude 259.23 km, has the larger node separation 0.748°. This is, in fact, the 481:30 repeat orbit, highlighted in Fig. 3. Therefore, to reduce the 61-day repeat grid into the 30-day one, it suffices to decrease the mean altitude by only 150 metres. The unstable nature of the 978:61 repeat orbit towards only a 50-cm disturbance in mean altitude is exhibited by the histograms in the lower panel of Fig. 5 (note the altitudes indicated above the bars).

By contrast, the near 61-day repeatability of orbits around the 977:61 orbit is preserved, even if the mean altitude is varied by ±100 m and ±200 m. The histograms of such orbits are shown in Figure 6, and correspond to

ACCEPTED MANUSCRIPT

neighbouring repeat configurations of 977:61 orbit in Fig. 3. In the case that the ion thruster should fail for a short time, an inevitable decrease in altitude due to air drag would follow, which for GOCE around 264-km altitude reaches 400–700 m/day. To have some safety margin, and in accordance with the planned 3–7-month duration of the measurement operational phases, a resonant configuration with a slightly higher mean altitude is worth consideration, e.g. the 75-day repeat orbit at 264.74 km.

Figure 6 should be positioned here.

Figure 7 should be positioned here.

The altitudes of resonant orbits, represented in Fig. 3, were calculated from Eq. (4). This equation was derived from secular changes in Eqs (1)–(3), the secular part of the *first approximation* of the full J_2 problem, and is accurate only to first order in J_2 (Klokočník et al., 2003). The mean altitudes calculated from Eq. (4) have an inherent uncertainty of, say, hundreds of metres. While in case of higher 977:61 orbit, the groundtrack repeatability is retained for such a deviation, for the lower 978:61 orbit much smaller departures from the exact value of the appropriate mean altitude lead to inhomogeneity in the groundtrack grids and, possibly, to shorter repeat periods.

Accepted Manuscript

ACCEPTED MANUSCRIPT

3.2.2. Histograms based on numerical orbit integrator

Although the simple J_2 analytical theory is good enough for providing a useful approximation to orbital motion of real satellites from both theoretical and practical aspects, when other orbital perturbations described in Sec. 2.1 are taken into account, the simulated orbits do differ from the analytical ones, especially during a single satellite revolution. We also take into account the lateral components of the drag, the dominant along-track drag component being balanced by the onboard ion thruster. In Figure 7, we show the histograms for several orbits near the higher 977:61 resonance. The original narrow bars from analytical theory (Fig. 6) become much wider, but still the bars are single-peaked around the theoretical 977:61 node separation, $\Delta\lambda$=0.3685°. The somewhat longer integration time of 65 days ensures that the histograms in Fig. 7 contain no bars located higher than at 0.4°. It is interesting that the mean altitude 263.9 km calculated from the J_2 analytical theory for the 977:61 resonant orbit (Fig. 6) is still valid in more realistic numerical integration for approximately 61-day repeat orbit (Fig. 7).

Let us remark here that the resonant orbits *above* the 16:1 resonance in Figure 3 are symmetrical with respect to the 16:1 mean altitude (Klokočník et al., 2008, Fig. 15), so the analysis in this section of the lower and higher example 61-day repeat orbits, closest to 16:1 altitude, is also valid 'from above', with the two orbits interchanged.

ACCEPTED MANUSCRIPT

4. Conclusions and suggestions for GOCE

In Section 2 we studied the early orbit phase of GOCE, when the satellite is let in a controlled free fall from the injection altitude of 280 km down to the first measurement phase altitude of around 264 km (Fig. 1). The anticipated passage through the strong resonance 16:1 at 268.4 km leads to changes in orbital elements, especially to the quasi-secular drift in inclination, which may reach $\pm 0.03°$. Recall that using the onboard ion thruster GOCE can only adjust its semimajor axis. As inclination and semimajor axis are key parameters in both sun-synchronicity and repeatability conditions, and after the passage through 16:1 resonance the inclination will be perturbed and may take some value differing from $96.7°$, it would be advisable to re-adjust the semimajor axis according to the actually measured values of inclination to ensure at best the orbit requirements, *after* the satellite will have passed through 16:1 resonance.

In Section 3, we analyzed some properties of near-repeating orbits suitable for GOCE measurement operational phases. We selected two 61-day repeat orbits as examples, the higher 977:61 orbit at 263.9 km, and the lower 978:61 orbit at 259.4 km (Fig. 3). After the repeat period of 61 days is completed, the groundtrack grids of both example orbits should theoretically be almost the same, with homogeneous coverage and equatorial node separation of 41 km. We show in Figure 4 that while the groundtrack grid pertaining to the higher 977:61 orbit covers the Earth's surface consecutively, that of the lower 978:61 orbit is laid down in two 30-day phases, each time a shifted half-density grid is created. Varying the mean altitudes by small steps around the exact resonance value for the two example orbits, we found their rather

ACCEPTED MANUSCRIPT

different behaviour in theoretical as well as practical aspects. The double-peaked shape of the histograms of node separation for orbits near the lower 978:61 repeat orbit (Fig. 5) show clearly that the orbit looses the exact repeatability character already with a 50-cm variation (Fig. 5, lower panel) and that a 150-metre decrease in mean altitude reduces the repeat period from 61 days to 30 days (upper panel). To the contrary, the histograms of orbits neighbouring the higher 977:61 repeat orbit are single-peaked and, therefore, these orbits retain their repeating character even if the mean altitude is varied by ± 200 m (Fig. 6). The conservation of the repeatability character for the higher 977:61 orbit towards a few hundred metres variations were tested using the full numerical integration, the narrow histogram peaks obtained from the analytical computations became broadened (Fig. 7). We would, therefore, suggest that, from the point of view of repeatability conservation towards the mean altitude variations, the repeat orbit for the GOCE measurement operational phases be located on the upper branch of resonant orbits in Fig. 3, which contains the 977:61 configuration. Due to variations in semimajor axis, or to a possible short-term failure of the onboard ion thruster, an orbit of slightly higher mean altitude might be advisable, which would have, say, 75-day repeat period and an altitude of 264–265 km.

Let us, finally, note one practical lesson learnt from the simulations of Section 3. A simple way for finding the value of mean altitude that ensures the near repeatability condition to be fulfilled, when one is interested in the modelling of *real orbital conditions* using the full numerical integrator, is to use the given (or measured) values of osculating elements, to make the integrator predict orbits for an appropriate range of semimajor axis values,

ACCEPTED MANUSCRIPT

and to draw the histograms of node separation, which show the repeatability character of the orbit considered (like Fig. 7). The ion thruster may then be used to adjust the semimajor axis to the chosen optimum value.

5. Acknowledgements

The authors are grateful to an anonymous reviewer for detailed comments and helpful suggestions. This work was supported by the ESA/PECS grant C 98056.

References

Biesecker, D. A., and the Solar Cycle 24 Prediction Panel, 2008. Solar Cycle 24 Prediction Panel Update. Space Weather Workshop, 29 April–2 May, Boulder, Colorado, USA.

Brouwer, D., 1959. Solution of the problem of artificial satellite theory without drag. Astron. J. 64, 378–397.

Colombo, O. L., 1984. Altimetry, orbits and tides. NASA Tech. Memo., NASA TM-86180.

Drinkwater, M. R., Haagmans, R., Muzi, D., Popescu, A., Floberghagen, R., Kern, M., Fehringer, M., 2007. Proceedings of 3rd International GOCE User Workshop, 6–8 November, Frascati, Italy, ESA SP-627.

ESA, 1999. Gravity Field and Steady-State Ocean Circulation Mission, report for mission selection of the four candidate Earth Explorer missions. ESA SP-1233(1).

Accepted Manuscript

ACCEPTED MANUSCRIPT

ESA, 2004. GOCE Ground Segment Concept and Architecture, GO-TN-ESA-GS-0017.

Gooding, R. H., Wagner, C. A., Klokočník, J., Kostelecký, J., Gruber, C., 2007. CHAMP and GRACE resonances, and the gravity field of the Earth. Advances in Space Research 39, 1604–1611.

Hairer, E., Nørsett, S. P., Wanner, G., 1993. Solving ordinary differential equations I. Nonstiff problems. Springer.

Hofmann-Wellenhof, B., Moritz, H., 2006. Physical Geodesy. Physical Geodesy. ISBN 3-211-33544-7, Springer, Berlin.

Kaula, W. M., 1966. Theory of satellite geodesy. Applications of satellites to geodesy. Waltham, Mass.: Blaisdell.

King-Hele, D. G., 1992. A Tapestry of Orbits, ISBN 052139323X, Cambridge University Press.

King-Hele, D. G., Winterbottom, A. N., 1994. Comparison of geopotential harmonics in comprehensive models with those derived from satellite resonance, 1972-1993. Planet. Sp. Sci. 42, 359–365.

Klokočník, J., Kostelecký, J., Gooding, R. H., 2003. On fine orbit selection for particular geodetic and oceanographic missions involving passage through resonances. Journal of Geodesy 77, 30–40.

Klokočník, J., Wagner, C. A., Kostelecký, J., Bezděk, A., Novák, P., McAdoo, D., 2008. Variations in the accuracy of gravity recovery due

Accepted Manuscript

ACCEPTED MANUSCRIPT

to ground track variability: GRACE, CHAMP, and GOCE. Journal of Geodesy, 22–32.

NOAA, 2007. Next solar storm cycle will start late. Press release, April 25, http://www.swpc.noaa.gov/SolarCycle/SC24/PressRelease.html.

Parke, M. E., Born, G., 1993. The effects of altimeter sampling characteristics: Some Geosat examples. Naval Research Lab. Report.

Parke, M. E., Stewart, R. H., Farless, D. L., Cartwright, D. E., 1987. On the choice of orbits for an altimetric satellite to study ocean circulation and tides. J. Geophys. Res. 92, 11693–11708.

Tapley, B. D., Schutz, B. E., Born, G. H., 2004. Statistical Orbit Determination. Elsevier Academic Press.

Zarrouati, O., 1987. Trajectoires Spatiales. Cepaudes-Editions, Toulouse.

Accepted Manuscript

ACCEPTED MANUSCRIPT

443 ## Figure captions

Figure 1: Mean orbital elements calculated by NUMINTSAT (GOCE free-fall simulation; start: 10 Nov 2008).

Figure 2: Histograms of gravitational and nongravitational accelerations in the local reference frame components (simulation for GOCE, 10/2008–10/2009, altitude 263.9 km).

Figure 3: Orbital resonances predicted for GOCE (inclination 96.7°).

Figure 4: Evolution of groundtrack grid for resonant orbits 977:61 and 978:61. Only a subsection of the ascending parts of the orbit is drawn.

Figure 5: Histograms of node separation for orbits near the 978:61 resonance as function of the mean altitude (which is indicated above the bars). The data were calculated using the J_2 analytical theory.

Figure 6: Histogram of node separation for orbits near the 977:61 resonance. The data were calculated using the J_2 analytical theory.

Figure 7: Histogram of node separation for orbits near the 977:61 resonance. The simulated data from 65 days using the EGM 2008 geopotential up to degree/order 50 and all orbital perturbations depicted in Fig. 2.

Accepted Manuscript

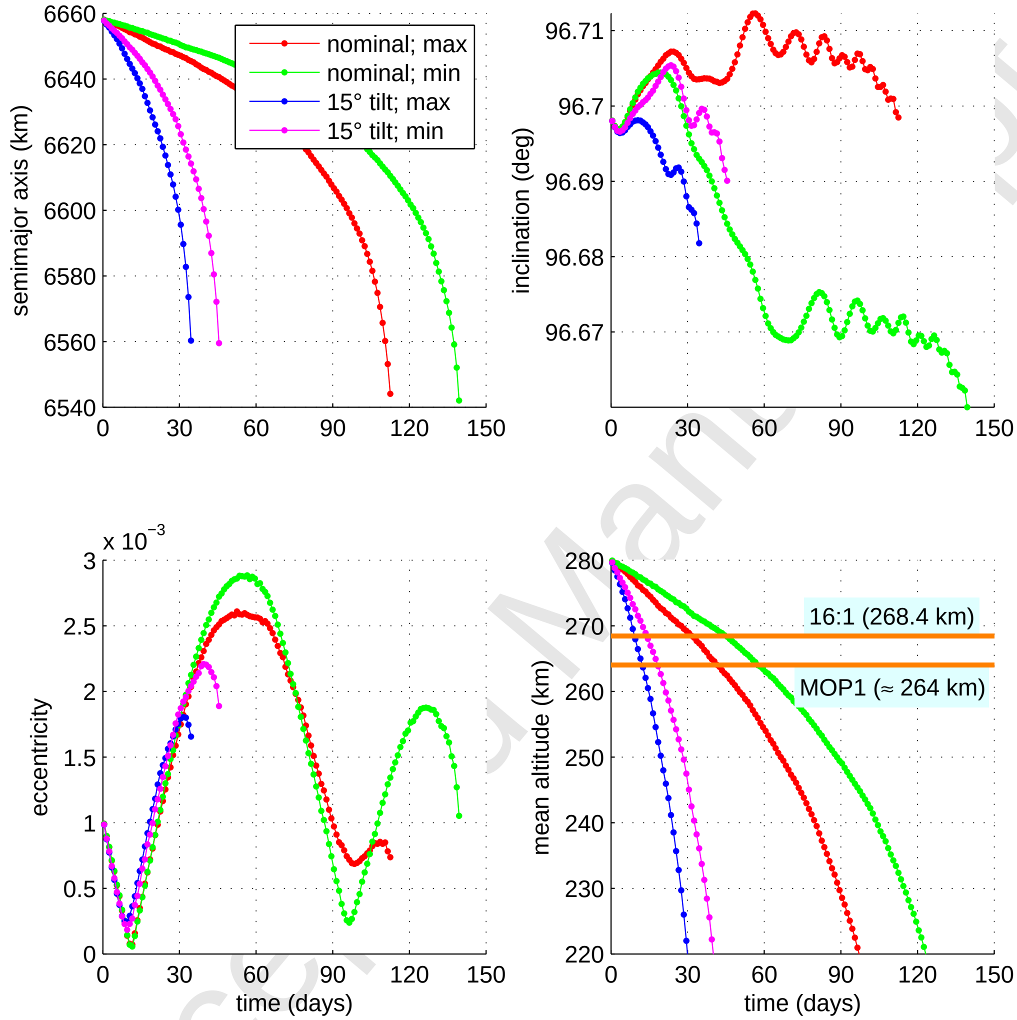

Figure 1

Accepted Manuscript

ACCEPTED MANUSCRIPT

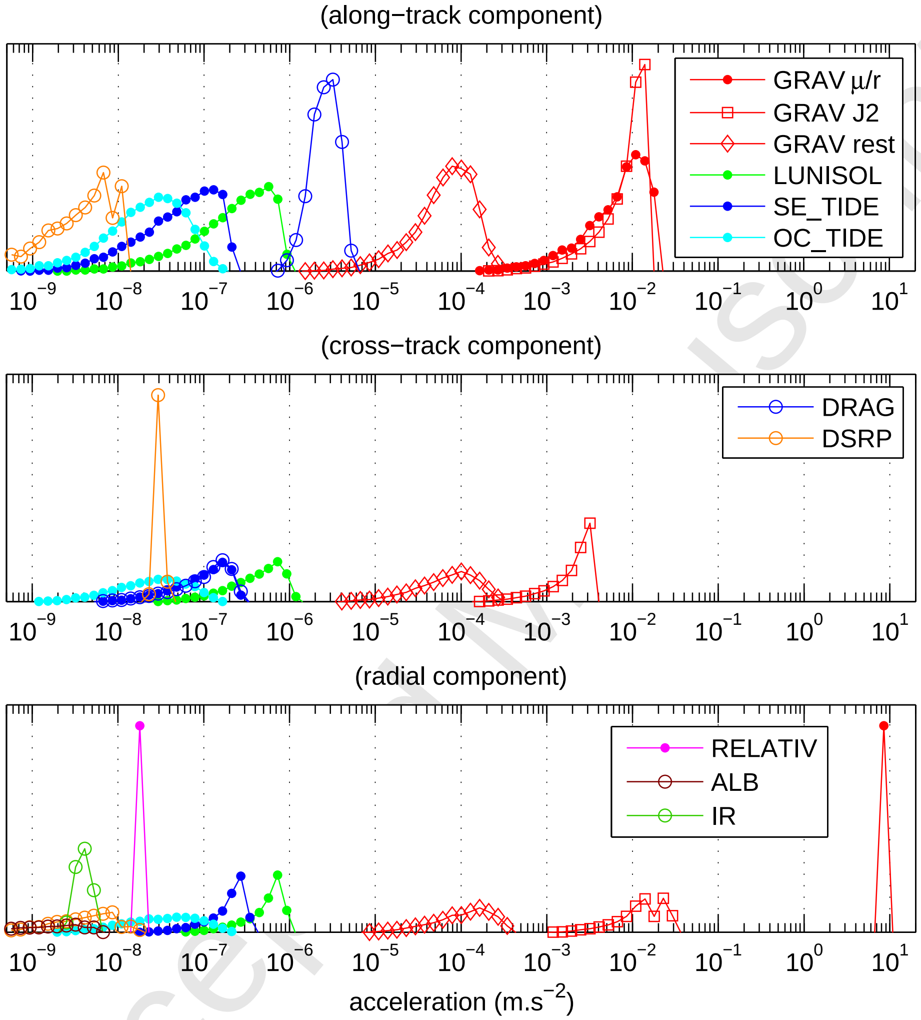

Figure 2

Accepted Manuscript

ACCEPTED MANUSCRIPT

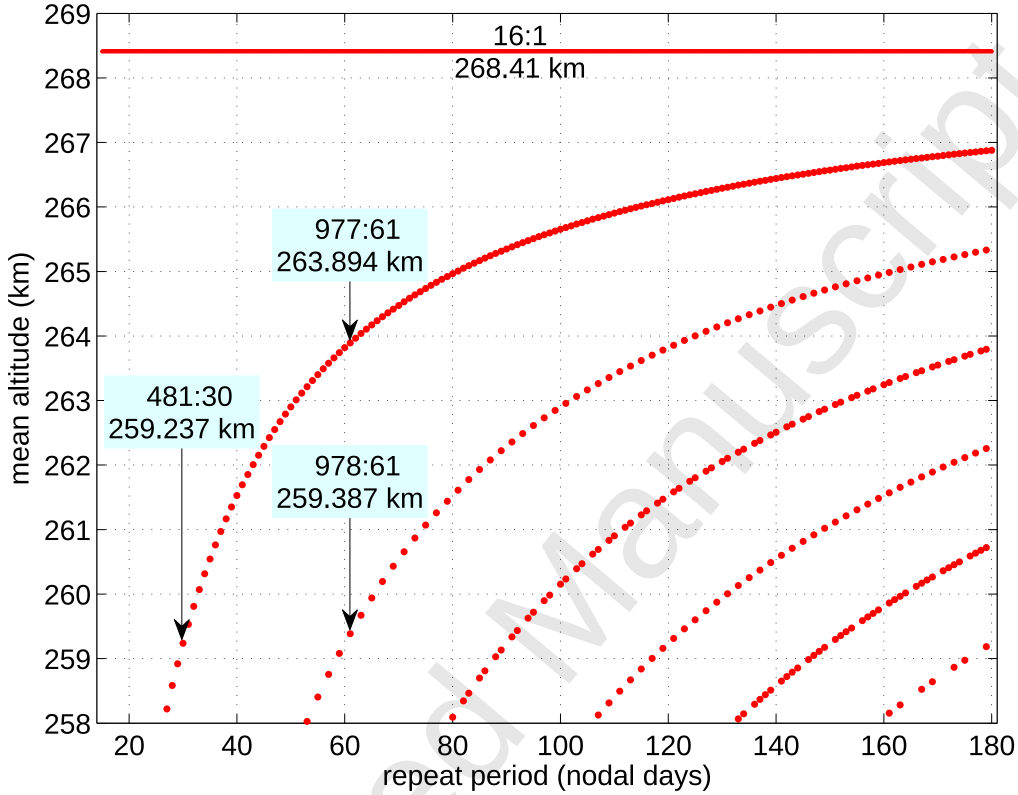

Figure 3

Accepted Manuscript

450

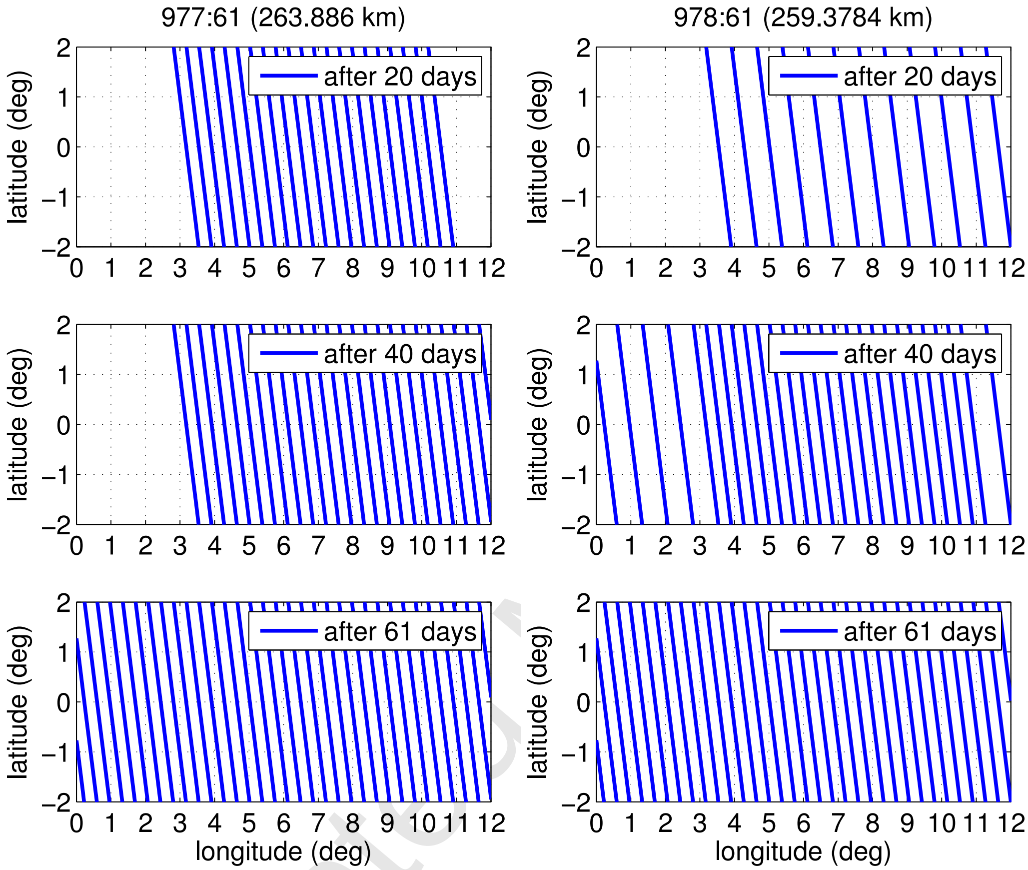

451 Figure 4

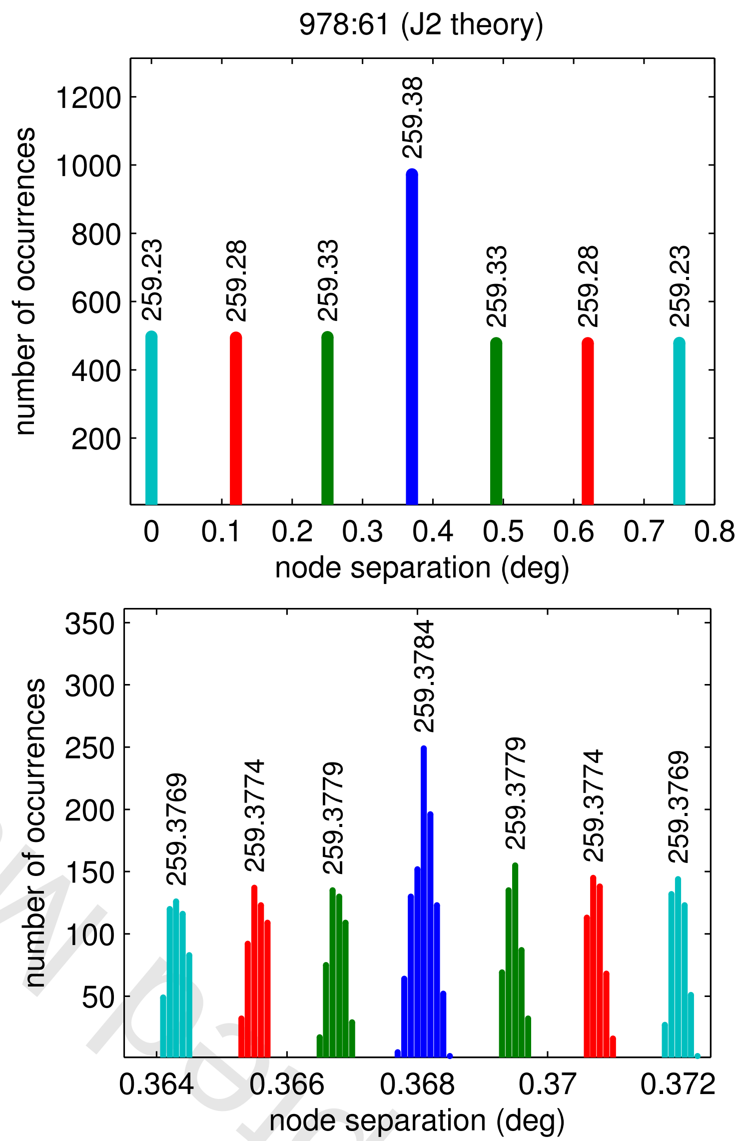

Figure 5

Accepted Manuscript

ACCEPTED MANUSCRIPT

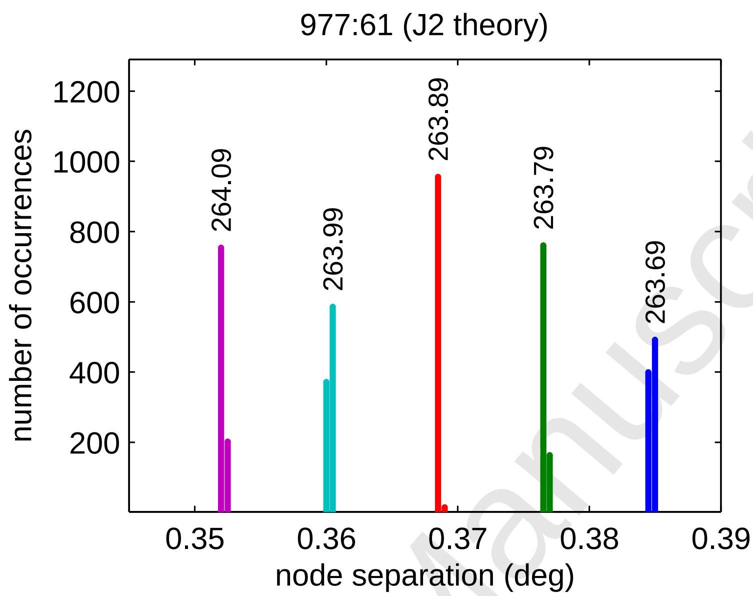

Figure 6

Accepted Manuscript

ACCEPTED MANUSCRIPT

456

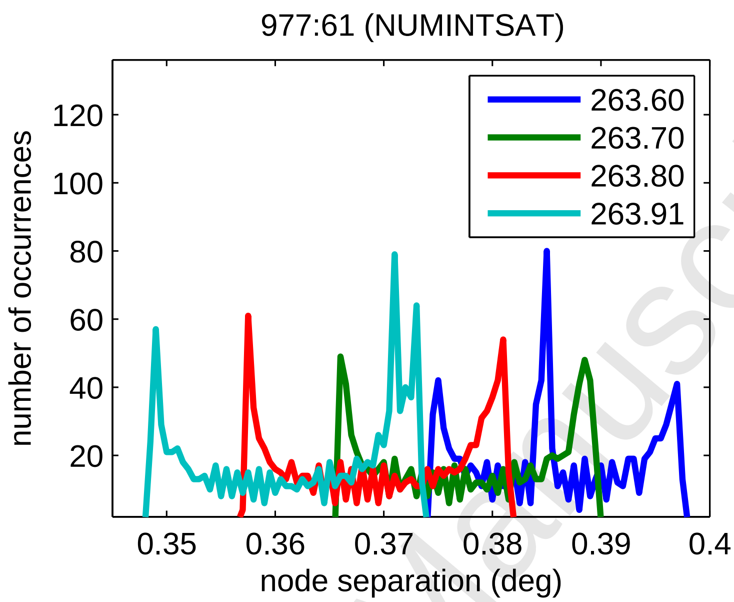

457 Figure 7

Accepted Manuscript